Author Version: *J. Geophys. Res. (C: Oceans): 116(6); 2011; doi:10.1029/2010JC006603, 17 pp*

Observational evidence of lower frequency Yanai wave in the central equatorial Indian Ocean

Divya T. David[1], S. Prasanna Kumar[*1], P. Byju[1], M.S.S. Sarma[1], A. Suryanarayana[1], V.S.N. Murty[2]

[1]National Institute of Oceanography, Council of Scientific and Industrial Research (CSIR), Dona Paula, Goa-403 004, India.

[2]National Institute of Oceanography, Council of Scientific and Industrial Research (CSIR), Regional Centre, 176, Lawsons Bay Colony, Visakhapatnam-530 017, India.

Abstract

The analysis of long time-series current meter data from a mooring at 77^0E and equator during 2003-2007 along with mean sea level anomaly (MSLA) data throws light on the occurrence of the lower frequency Yanai wave (24-40 day) in the upper water column of the central equatorial Indian Ocean (EIO) during the positive Indian Ocean Dipole (IOD) years of 2003, 2004, 2006 and 2007 and its absence during the negative IOD year of 2005. This result is in contrast with the earlier studies that observed only the higher frequency (biweekly period) Yanai wave in this region. We propose a new notion for the generation of the lower frequency Yanai wave in the upper central EIO due to the positive IOD phenomenon. The strong meridional current shear created by the northward shifting and strengthening of the westward flowing south equatorial current (SEC) associated with positive IOD and the eastward flowing southwest monsoon current provides energy for the generation of lower frequency Yanai waves. The vertical stratification of the water column appears to be responsible for the trapping of different frequency of Yanai wave with only the higher frequency Yanai wave in the region of lower pycnocline. During positive IOD the strongly stratified upper water column responds to the lower frequency Yanai wave while the deeper ocean (4000m) exhibited longer period (47-day) oscillation. The expected surface signature of Madden-Julian Oscillation (MJO) seems to be suppressed by strong easterlies during the positive IOD years.

---

* Corresponding author

1. Introduction

The intraseasonal oscillations (ISO) that vary from 10 to 100 days [*Lau and Waliser*, 2005] are crucial and integral part of the weather and climate events. They play a key role in initiating events such as El Nino [*McPhaden*, 1999] and influence the weather at extratropical latitudes [*Bond et al.*, 2003; *Jones et al.*, 2004]. In the ocean there are internally as well as externally generated ISO [*Sengupta et al*., 2001, *Waliser et al*., 2003; *Miyama et al*., 2005; *Han*, 2005]. The former arises due to instabilities of mean current system having an average period of about 20-30 days [*Kindle and Thompson*, 1989; *Woodberry et al*., 1989], while the latter arises due to atmospheric wind forcing such as active and break spells of monsoon rainfall [*Sengupta et al*., 2001], MJO (30-60 days) [*Madden and Julian*, 1972; *Miyama et al., 2005*], quasi-biweekly mode (10-18 days) [*Miyama et al., 2005*] and 90-day winds (basin resonance) [*Han*, 2005]. The ISO in the tropical atmosphere such as the westward propagating Rossby waves, eastward propagating Kelvin waves [*Wheeler and Kiladis*, 1999; *Chatterjee and Goswami*, 2004], the quasi-biweekly mode (QBM) [*Murakami and Frydrych*, 1974; *Chen and Chen*, 1993; *Numaguti*, 1995] and their impact on the monsoon activity and El Nino events [*Lau and Chan*, 1988; *Long and Li*, 2002] are extensively studied. In the ocean, however, studies on ISO are mostly confined to the lower frequency (30-100 days) [*Madden and Julian*, 1971, 1972; *Hirst and Lau*, 1990; *Wang and Xie*, 1998; *Yu and Liu*, 2001; *Duvel and Vialard*, 2007; *Sobel et al.*, 2008], and most of them are based on theoretical analysis, statistical methods and numerical simulations. There is paucity of observational analysis available on the activity and pattern of ISO in the Indian Ocean [*Sengupta et al*., 2001*; Li et al.,* 2005] especially at the lower end of the spectrum, i.e., 10-30 days. Among the higher frequency ISO, the Kelvin and Yanai (named after its discoverer M. Yanai, 1966 first in stratosphere) waves are the only two waves seen in 10-30 days. Of these, the Yanai wave is unique as it has no counter parts at higher latitudes and is the least studied.

The 25-28 day (lower frequency) Yanai waves are prominently observed in the eastern equatorial regions of Pacific [*Harvey and Patzert*, 1976; *Wunsch and Gill*, 1976; *Legeckis,* 1977; *Cox*, 1980; *Ripa and Hayes*, 1981] and Atlantic Oceans [*Weisberg et al.,* 1979; *Weisberg and Horrigan*., 1981] and in the western region of Indian Ocean [*Luyten and Roemmich,* 1982; *O'Neill*, 1984; *Reverdin and Luyten*, 1986; *Woodberry et al.*, 1989; *Moore and Mccreary*, 1990; *Tsai et al*., 1992; *Kelly et al.*, 1995]. Yanai waves whose period varies between a week and a month [*McPhaden*, 1982; *Moore and Mccreary*, 1990] exhibit the gravity wave characteristics at higher frequencies and Rossby wave characteristics at lower frequencies and hence the name Mixed Rossby Gravity (MRG) wave. They are antisymmetric about the equator i.e., antisymmetric in zonal current velocity and symmetric in

meridional current velocity [*Wunsch and Gill,* 1976]. The energy propagation of MRG wave is in eastward and downward directions, while its phase propagation can be in eastward (higher frequency wave) or westward (lower frequency wave) directions [*Tsai et al*., 1992, *Sengupta et al*., 2004] and vertically in the upward direction. They play a major role in the heat and momentum balance of the equatorial oceans [*Kelly et al.*, 1995].

Luyten and Roemmich [1982] was the first to observe a 26-day period variability in the meridional current from the current meter mooring in the western equatorial Indian Ocean (EIO) (40^0E-60^0E longitude). Later *Reverdin and Luyten,* [1986] identified these to Yanai waves based on both current meter and drifting buoy data from the same region. Several theories were put forward to explain the generation of Yanai wave which includes the reflection of incoming equatorially concentrated meridional kinetic energy by the slanting African coast [*O'Neill*, 1984], instability associated with the northward shift of the southern gyre during later stages of southwest monsoon [*Reverdin and Luyten*, 1986], and action of cross equatorial winds on the slanted coastline of the western boundary [*Moore and Mccreary*, 1990; *Kelly et al.*, 1995]. However, *Tsai et al*. [1992] did not subscribe to the idea of direct wind forcing of Yanai wave as they did not see a corresponding periodicity in the wind. *Kelly et al.* [1995] suggested that the unstable and meandering eastward current driven by the oppositely flowing Somali current and East African coastal current during northeast monsoon resonantly force the Yanai wave of the southwest monsoon. All the above studies indicated the strongest and coherent signals of Yanai waves in the western EIO during July-September period. However, their eastward propagation was partially blocked by Maldives island chain located between 73^0E and 74^0E [*Woodberry et al.*, 1989].

In contrast to western EIO, a biweekly period MRG wave (average period of 14-day) triggered by direct wind forcing of almost the same period is observed in the eastern EIO (80^0E-100^0E longitude) [*Schott et al*., 1994; *Reppin et al*., 1999; *Murty et al*., 2002; *Sengupta et al.*, 2001, 2004]. This biweekly oscillation is prominent in the upper 100m, while the 20-30 day variability is seen below 125m at 90^0E [*Masumoto et al.*, 2005]. *Miyama et al.* [2005] simulated an eastward intensification of energy due to the reflection of Yanai wave packet from the near-surface pycnocline and bottom and suggested that, since there are no free equatorial waves having the same period with westward group speed, part of the energy of the biweekly wave can escape to higher latitude via coastal Kelvin waves.

A possibility of less than 20-day variability at the central EIO (60^0E-80^0E) was first suggested by *McPhaden* [1982] from the weekly record of current at Gan Island (~73^0E). The prominent biweekly

variability in the near ocean surface in the modeling studies of *Sengupta et al*. [2001] and *Miyama et al.* [2005] is a result of direct wind forcing. *Ogata et al.* [2008] attributed the generation of a 20-70 day oscillation below 150m at south east of Sri Lanka during boreal autumn and early winter to the large barotropic energy conversion.

From the above discussion it is evident that studies of MRG wave in the central EIO are very few compared to western and eastern equatorial Indian Ocean. The earlier studies came up with the view that the lower frequency Yanai wave oscillation is dominant in western equatorial Indian Ocean while higher frequency oscillation in a biweekly scale prevailed in the central and eastern equatorial Indian Ocean in the upper water column. The lower frequency oscillations were observed only at the subsurface in the central equatorial Indian Ocean and eastern equatorial Indian Ocean [*Ogata et al*., 2008]. The higher frequency MRG wave (6-18 day) characteristics above the thermocline depth as well as at 4000m depth have been studied earlier in detail at central and eastern equatorial Indian Ocean [*Ogata et al*., 2008].

In the present study we use for the first time a long time-series current data spanning five years from the central equatorial Indian Ocean to explore the presence of Yanai wave. We followed a sampling strategy of high vertical resolution in the upper 150m and low resolution below. Unlike the earlier studies, where the upper ocean was sparsely sampled for short duration and the data for the entire sampling period were analyzed as a whole [*Mcphaden, 1982; Schott et al., 1994; Reppin et al., 1999; Murty et al., 2002*], we analyzed the long-term data for the entire period as well as for each separate years to decipher the occurrence of the lower frequency Yanai wave in the upper layer of the central equatorial Indian Ocean and propose a mechanism for its generation. Section 2 deals with the data and section 3 describe the methodology used for analyzing the data sets. The results are presented in section 4 and discussion part in section 5. The summary and conclusions are given in section 6.

2. Data

In the present study we used a host of data sets which includes both in situ as well as remote sensing data.

2. 1. In situ data

Two types of in situ data were used for the present study, the current data and the temperature and salinity data. The current data were obtained from Acoustic Doppler Current Profiler (ADCP) and

Recording Current Meters (RCM). The temperature and salinity data were from Array for Real-time Geostrophic Oceanography (Argo).

2.1.1 Current data and quality control

The in situ ocean current data used for the present study is obtained from deep sea current meter moorings deployed by National Institute of Oceanography (NIO, India) in the EIO since 2000 with the objective to generate long term time-series data for understanding the dynamics of the equatorial currents in relation to climate variability and change [*Murty et al*., 2005]. Aanderaa Recording Current Meters (RCM) were maintained at six nominal depths with the help of a mooring to study currents in the upper thermocline (100m), main thermocline (300m), intermediate waters (500m and 1000m), deep water (2000m) and near bottom water (4000m) respectively. Three deep sea current meter moorings of this type were deployed at 77^0E, 83^0E and 93^0E longitudes. From 2004 onwards an upward looking ADCP was placed at a nominal depth of 100m at each of the mooring. The current data at 77^0E, equator was analyzed (Table 1, Figure 1) in the present study which consisted of ADCP data for the period 19 October 2004 to 25 June 2006 and RCM data during the period 12 September 2003 to 6 December 2007. See Table 1 for details on the deployment-recovery cycle, data availability and data gaps. It is worth noting that the period of the time-series data used in the present study includes four positive IOD years of 2003, 2004, 2006 and 2007 and a negative IOD year of 2005. The RCM provided hourly data of temperature, salinity, current speed and direction. From the hourly RCM data the hourly zonal and meridional current velocities were derived, which were subsequently averaged to obtain daily mean (Auxiliary Figures 1 to 3). The ADCP provided zonal and meridional current velocities at 15 minute interval and 4 meter depth bins which were converted to daily mean 8m depth bin data (Auxiliary Figure 4). A continuous time-series data was generated from the daily RCM data by linearly interpolating the data gaps, which were typically on an average of 4 days, except at 500m during May 2005 which was 15 days. The entire data at 300m during 2004-05 and at 2000m during 2003-04 and 2006-07 were not used for the analysis as it had large data gaps (see Table 1 and Figure 1 for details). The “bad values” in the ADCP data were eliminated and the data gaps, which were typically on an average of 6 days were linearly interpolated for further analysis (see Table 1 for details).

2. 1. 2. Argo data

The annual mean temperature, salinity and density profiles were obtained from the daily Argo data for the Indian Ocean basin from 2003 to 2007 to study the vertical hydrographic characteristics of the water column during the period of study.

2. 2. Remote sensing data

In addition to the above mentioned in situ data we have also used remote sensing data. To delineate the years of IOD during the observational period the weekly Dipole Mode Index (DMI) was examined using data from January 2003 to December 2007 derived from National Oceanic and Atmospheric Administration Optimum Interpolation Sea Surface Temperature Version 2 (NOAA OI SST Ver.2). This DMI is the weekly anomalous sea surface temperature (SST) gradient between western equatorial Indian Ocean (50^0E-70^0E and 10^0S-10^0N) and south eastern equatorial Indian Ocean (90^0E-110^0E and 10^0S-0^0N). Positive and negative DMI represents positive and negative IOD respectively. The surface (15m depth) pentad current data from Ocean Surface Current Analyses - Real time (OSCAR) having 1^0 x 1^0 resolution [*Bonjean et al.,* 2002], daily wind data from ocean surface winds derived from sea wind Quick Scatterometer (QuikSCAT) with 0.25^0 x 0.25^0 resolution and weekly MSLA data with a resolution of 0.33^0 x 0.33^0 from delayed time global reference merged data set from Jason-1, Jason-2 and Topex Poseidon (T/P) were used to understand the variability associated with the upper ocean.

3. Methodology

The time-series data from the ADCP, RCM, MSLA and wind were analyzed using Variance Preserving analysis (VP) [*Emery and Thompson,* 1997]. Further the peaks with 95% and above confidence level (CL) have been determined using the Chi-squared distribution (CS) [*Emery and Thompson,* 1997]. The Continuous Wavelet Transformation (CWT) [*Addison*, 2002] was carried out on the meridional current velocity from the ADCP and RCM to understand the temporal variation of the Yanai wave period. Morlet wavelet was used as the mother wavelet. To aid further analysis, the westward propagating part of the Yanai wave of period 7-40 day was equally divided into higher frequency (7-23 day) and lower frequency (24-40 day) spectrum based on the frequency analysis (of the present current meter data as well as by previous authors) that showed distinct spectral peaks centered at 19-day and 26-day.

The temperature and salinity profiles from Argo data for central EIO within a 2-degree longitude by 2-degree latitude box centered at 77^0E and equator (i.e., from 76^0E to 78^0E longitude and 1^0N to 1^0S latitude) were extracted for the years from 2003 to 2007. From the total number of profiles available for each year (Table 2) the annual mean temperature and salinity profiles were computed which were subsequently used for the computation of sigma-t. The static stability parameter was calculated following *Pond and Pickard* [1983] to assess the strength of stratification.

To explore the existence of lower frequency Yanai waves in the EIO, the region between 3^0N and 3^0S was further divided into 3 boxes such as western (50^0E-60^0E), central (70^0E-80^0E) and eastern (90^0E-100^0E) (Figure 2).

4. Results

4. 1. ADCP data

As the Yanai wave signatures can be easily inferred from the meridional current velocity, which is symmetric about the equator [*Wunsch and Gill*, 1976], the significant peaks with 95% and above confidence level (CL) were identified using CS (Table 3) analysis carried out on the daily meridional current velocity obtained from the ADCP data at 77^0E, equator for the period 19 October 2004 to 25 June 2006 at each depth from 48m up to 120m. The 26-day peak was observed significant along with the biweekly peak of 12-day in the upper 88m of the water column, while the higher frequency Yanai wave peaks were observed towards deeper depths up to 120m (Table 3, also Auxiliary Figure 5). The 26-day and the biweekly were the lower and higher frequencies of Yanai wave. In order to understand the reason for such a depth differentiation of the prominent period of Yanai wave, the water column characteristics were analyzed.

As the number of Argo profiles are limited (Table 2), the annual mean profiles of salinity and temperature at 77^0E and equator were calculated from the Argo data and this showed a strong halocline/pycnocline in the upper 88m (Figure 3). The lower as well as higher frequency Yanai wave during 2003, 2004, 2006 and 2007 was observed in the upper thermocline/halocline/pycnocline region, which had an average density gradient of 0.0333, 0.0429, 0.0367 and 0.0368 kg/m^3 per meter respectively. During 2005, a 47-day peak was observed in this upper pycnocline region having an average density gradient of 0.0308 kg/m^3 per meter (the difference in density gradient during 2005 over the depth range 48-88m is larger than that of the IOD years), while the higher frequency Yanai wave alone was observed below the upper pycnocline (up to 120m) as in the case of the other years.

The higher frequency Yanai wave during 2003, 2004, 2005, 2006 and 2007 occurred distinctively within the lower pycnocline region (96-120m) which had an average density gradient of 0.0111, 0.0285, 0.0341, 0.0333 and 0.0347 kg/m^3 per meter respectively. The decrease in the density with depth would lead to an increase in the phase velocity of Yanai wave and decrease in its period. To explore this further, we calculated the stability of the water column during each year based on the mean profiles of temperature and salinity. The depth averaged static stability parameter shows that during the positive IOD years of 2003, 2004, 2006 and 2007 upper pycnocline (48-88m) is more strongly stratified and stable compared to the negative IOD year 2005 (Table 4). The difference of static stability parameter between the upper (48-88m) and lower (92-120m) pycnocline is the lowest during 2005 (- 153.3 x 10^{-6} m^-1). This difference in static stability is more than 2-times and 2½ -times during 2003 and 2004 respectively, while it is about 1.4 during 2006 and 2007. Thus, we see a close correspondence between the periods of the Yanai wave with the vertical distribution of the water column stability during positive IOD years.

To understand the temporal variability of the Yanai wave period, the ADCP data was further subjected to CWT analysis (Figure 4). Since Yanai wave showed a change in its period above and below 88m, the ADCP data was segregated into two depths by averaging (1) from 48m up to 88m depth and (2) from 96m up to 120m depth. This data was used for the CWT analysis. In the upper water column (48-88m) the highest energy (180-240 (cm^2/s^2)/day) was in the range of 24-34 day period during October to December, 2004 followed by 29-48 day period during November 2005 to January 2006, and 16-25 day period during end of January to February, 2006 (Figure 4, top panel). Note that there was no Yanai wave signature in 2005. Below 88m, highest energy was seen in the period 14-22 day during December 2004 to third week of January 2005 (Figure 4, bottom panel), followed by 13-19 day from August to September 2005, 12-24 day from last week of December 2005 to February 2006 and 28-40 day during January to April, 2006. The 29-48 day signature was seen (Figure 4, upper panel) in the upper 88m water column during the negative IOD year of 2005. This higher period (29-48 day) signature corresponds to the 47-day peak that we observed in CS and it shows similarity in both frequency and time of occurrence of MJO. Hence, it is reasonable to assume that the variability might be of MJO origin. Even though some energy corresponding to the 29-48 day signature was observed in the bottom panel of the CWT analysis of ADCP data, CS analysis showed that it was not significant. Hence only higher frequency Yanai waves were significant in 96-120m depth. The existence of higher frequency Yanai wave (below 88m) and the absence of lower frequency Yanai wave (both below and above 88m) are the notable features observed from the CWT analyses of ADCP data during the negative IOD year of 2005. An absence

of the higher period (47-day) signature in the depth range of either 48-88m or 96-120m during the IOD year of 2004 is also noted. To study the Yanai wave below the ADCP depth, further analysis was done with the RCM data.

4. 2. RCM data

4. 2. 1 Deployment-recovery period of 2003-04

The significant spectral peaks were determined using CS, which showed both higher and lower frequency Yanai wave at 150m and 300m depths, while only higher frequency Yanai wave at 500m and 1000m depths (Table 5). At 4000m depth only 47-day peak was significant and this period was not significant in any other depths. Note that a similar 47-day peak was prominent in the ADCP data during 2005. From the above analysis it is clear that the water column from 150 to 1000m depth responds to lower (28-day) and higher frequency (7-23 day) Yanai wave.

The temporal variation of various peaks obtained from the above analysis of RCM data was determined using CWT (Figure 5). At 150m, the highest energy was in 16-26 day period, which was seen during September-October, 2003 and April-May, 2004. At 300m, the highest energy was in 16-26 day and occurred only during November and December, 2003. The highest energy was seen at 20-30 day period during May and June at 500m, while it was at 22-35 day period in August, 2004. At 1000m depth the highest energy was seen at three different ranges, 11-20 day period in October, 2003 followed by 17-29 day period from November, 2003 to January, 2004 and 31-42 day period from October to December, 2003. The highest energy at 4000m was seen at 37-60 day from January to September, 2004.

4. 2. 2. Deployment-recovery period of 2004-05

The CS during 2004-05 (Table 5) exhibited 47-day and 16-day spectral peaks at 500m. At 2000m and 4000m only 47-day was seen significant. The lower frequency Yanai wave peak was not seen at any depth during this period. Thus, the MJO like oscillation was the significant mode of variability throughout the water column. The CWT analysis was done for delineating the time of occurrence of this variability. The CWT of 2004-05 (Figure 6) at 500m showed highest energy at 18-25 day period from November to first week of December, 2004 followed by 31-52 day period from July to October, 2005. The lower frequency Yanai wave was not discernible at any depth during this period. The highest energy at 2000m was in the range of 27-42 day from March to May, 2005 while at 4000m it was in the range of 30-49 day from December, 2004 to March, 2005. Unlike the previous years

(2003-2004) the signature of Yanai waves were not seen at any depth during 2005. The only signal that was seen prominent was in the 47-day period.

4. 2. 3. Deployment-recovery period of 2006-07

The presence of higher and lower frequency spectral peaks of Yanai waves were seen in the upper 1000m (Table 5). However, only the 21-day peak at 450m and 47-day peak at 4000m were found significant in the CS distribution (Table 5). The temporal variation of the above significant periods, examined using CWT (Figure 7), showed that at 450m the highest energy was in 12-35 day period, which occurred from the last week of February to the first week of April, 2007 followed by 28-40 day period from January to first week of April, 2007. At 550m the 30-54 day period exhibited the highest energy from December, 2006 to February, 2007 followed by 16-35 day period from January to May, 2007 and 16-40 day period from August to December, 2007. The 31-46 day period showed the highest energy at 800m which occurred from October to December, 2006 while the highest energy at 14-34 day period was observed from the last week of February to April, 2007. At 1000m, 13-22 day period had the highest energy in October, 2006 followed by 20-31 day period from January to May, 2007 and 14-30 day from August to November, 2007. The highest energy at 4000m was in 37-60 day period observed from December, 2006 to the first week of April, 2007 similar to the other deployment-retrieval periods. The Yanai wave signature was not seen at 4000m, which is consistent with earlier periods of 2003-04 and 2004-05.

Earlier studies showed that MJO signals are strong at the equator during boreal winter and spring while it is weak during summer [*Madden* 1986; *Gutzler and Madden*, 1989]. This seasonality is clearly seen in the CWT of RCM current measurements at 4000m. During 2003-04 the stronger 47-day signals are observed during January to August, 2004, while during 2004-05 (2006-07) stronger signals are seen during December 2004 (2006) up to April, 2005 (2007). In short, MJO like oscillations (47-day) were prominent at bottom waters during all the RCM deployment-recovery periods from 2003 to 2007. However, we do not know whether they are forced by atmospheric MJO or it is a resonant mode due to oceanic processes.

Thus, during positive IOD years the upper 1000m of the water column, except the lower pycnocline (96-120m), oscillates with a frequency of both lower and higher frequency Yanai wave, while during negative IOD year the response is mainly on 47-day period. The above analysis of the current data from ADCP and RCM as well as the temperature and salinity data from Argo profiles indicates a strong correspondence between the vertical stratification of the water column and the

depthwise presence of the Yanai wave and the 47-day oscillations at 77°E and equator. This has been depicted schematically in Figure 8.

5. Discussion

The above analysis brings out the following two important observations. The first one is the presence of the lower (24-40 days) as well as the higher (7-23 days) frequency Yanai waves in the upper 1000m of the water column at 77^0E and equator during all the years except 2005. The second is the presence of strong 47-day signature at 4000m during all the years from 2003 to 2007. The 47-day signature, with lower energy, observed from 500m upto 1000m in the CWT analysis during 2003-04 and 2006-07 RCM retrieval periods are not significant. During 2005, however, the 47-day signature is present in the entire water column, while the Yanai wave signature is absent, except in the depth range of 96-120m (where higher frequency Yanai wave is present). Thus, the year 2005 appears to be an anomaly and it is pertinent to explore what caused the suppression of lower frequency Yanai waves from the upper water column during 2005. Further, the existence of the higher frequency Yanai wave observed in the depth range of 96-120m during 2005 as well as all other years also would need an explanation. Since the meridional wind stress can effectively excite the Yanai/MRG waves [*Wunsch and Gill*, 1976], the QuikSCAT daily meridional wind stress for the central EIO between 75^0E-80^0E and equator from 2003 to 2007 were subjected to the CS and VP analysis (Figure 9 and 10). A biweekly peak in the intraseasonal time scale was seen during the entire period from 2003 to 2007 (Figure 9 and 10), it was significant only during 2003, 2005 and 2006 (Figure 9). This implies that the higher frequency component of the Yanai wave is from the direct atmospheric forcing. A similar result of the biweekly variability was obtained by *Sengupta et al*. [2001] and *Miyama et al.* [2005]. As the QuikSCAT wind did not show any significant energy peak in the 20-30 day period, ocean dynamics must be responsible for the observed lower frequency Yanai wave during 2003, 2004, 2006 and 2007.

In order to understand what caused the lower frequency Yanai wave during 2003, 2004, 2006 and 2007 we analyzed the SST DMI dataset, which showed that the year 2005 was a negative IOD year while the years 2003, 2004, 2006 and 2007 were positive IOD years (Figure 11). The annual mean and the mean for the months that showed positive DMI (February-March, September-December for 2004 and August, 2006 to January, 2007 for 2006) had the lowest positive values of 0.01 and 0.19 respectively for the year 2004, while the highest positive values of 0.35 and 0.88 respectively for the year 2006. Hence, the year 2004 is a weak positive IOD compared to that of 2003, 2006 and 2007.The year 2005 has the highest negative DMI with an annual mean of 0.33 (Figure 11). During

the positive IOD, which normally starts by May-June, peaks in October and quickly recedes during November-December, the stronger equatorial easterly winds cause a northward shift of the SEC (Figures 2 and 12a) compared to negative IOD year 2005 (Figure 12b). The northward shifted SEC, which flows westward, meets the eastward flowing southwest monsoon current at the central equatorial region (see Figure 2 for October, 2006) and generates a strong current shear across the equator (Figure 12c). Similar strong current shear was seen during the years 2003, 2004 and 2007 (figures not presented). This current shear is expected to generate stronger barotropic instability, while the vertical current shear associated with the cross-equatorial current shear is expected to generate baroclinic instability. Hence, we calculated the barotropic and baroclinic conversion rates following *Jochum et al*. [2003] using the OSCAR current data. Though the OSCAR current is at 15m depth, the calculated conversion is expected to hold good within the Ekman layer depth which ranged from 33m to 70m (average 51.5m, Auxiliary Figure 9). During most part of the study period the Ekman layer was deeper than 48m, especially during the period of formation of Yanai waves in a positive IOD period. The barotropic and the baroclinic conversions are given by $-\rho_o(\overline{u'v'})U_y$ and $(-g\,\overline{\rho'w'})$ respectively where ρ_o is the density of sea water, $\overline{u'v'}$ is the mean of the product of *u'* and *v'*, the deviations from the annual mean zonal and meridional current velocity for the period of May-November respectively, U_y is the zonal current shear, *g* is the acceleration due to gravity, and $\overline{\rho'w'}$ is the product of ρ' and *w*', the deviations from the annual mean density and vertical current velocity (calculated from the zonal and meridional current velocities) for the period of May-November respectively. The conversion rates are calculated for the central EIO [3^0N-3^0S latitude and 75^0E-80^0E longitude] (see Figure 2 for location) for each year. The barotropic energy conversion is positive during the positive IOD years (2003, 2004, 2006 and 2007) and indicates high eddy kinetic energy (EKE) (Fig.12d), which is the result of a net energy transfer from mean kinetic energy (MKE) and presence of Yanai waves. The higher negative value of barotropic energy conversion during 2005, which is a negative IOD year, implies a high MKE and absence of Yanai waves. The baroclinic energy conversion is 4-5 times higher than the barotropic energy conversion during 2003, 2006 and 2007, while it is more or less the same during 2004. However, during the year, 2005 the baroclinic energy conversion was close to zero. Thus, the cross-equatorial current shear during positive IOD years are able to generate high eddy kinetic energy, while the vertical current shear sustains the growth of eddy kinetic energy through higher baroclinic energy conversion. The above results are consistent with the results from the spectrum analysis which showed that Yanai waves in 2005 were weak. Hence we propose that the above processes during a positive IOD create a situation conducive for the generation of the lower frequency Yanai waves.

Now let us examine what would have prevented the expected MJO signals to be dominantly present in the upper 1000m during positive IOD years. The strong equatorial easterlies during the positive IOD along with cold SST suppress the eastward propagating MJO signature and weaken it. In addition, the upper pycnocline was strongly stratified and stable during the positive IOD years in comparison to the negative IOD year of 2005. This was due to the advection of low salinity waters from the east by the northward shifted SEC (see Fig.3 for a comparison of salinity between positive and negative IOD year). We presume that the strong vertical stratification prevented the upper water column to be dominantly in resonance with MJO which is weak. However, there may be some weak response. Thus, during positive IOD years the upper water column dominantly resonates at the Yanai wave frequency due to the increased meridional shear and vertical stratification, while the deeper waters exhibit 47-day oscillations. During negative IOD year when the water column is weakly stratified the entire water column exhibit 47-day oscillations.

In order to see whether the Yanai wave signatures were perceptible in the surface layer above the depth of measurement of ADCP, the merged MSLA data was analysed. Since both the Yanai waves and Kelvin waves are present in the MSLA data in the 14-30 days range, to delineate the Yanai wave signature alone it is necessary to use its characteristic property. As the sea level for the Yanai wave is antisymmetric about the equator [*Meyers et al.,* 1993] we converted the sea level field, $h(x, y)$ to symmetric and antisymmetric components, and then used the antisymmetric sea level anomaly, h_A for further analysis.

$$h_{A\,(x,y)} = {}^{1}/_{2}\,[h_{(x,y)} - h_{(x,-y)}]$$

where x and y are the longitude and the latitude respectively. Since maximum variance of Yanai wave were seen at 3^0 latitude in both hemispheres in EIO [*Tsai et al*., 1992] the antisymmetric MSLA, after removing the seasonal cycle, were used to calculate the CS for western, central and eastern EIO (Figure 13) for the same time period as that of ADCP measurement.

The CS of the antisymmetric MSLA after removing the seasonal cycle in the western and central EIO clearly showed a spectral peak at 28-day (Figure 13). In addition to this a 17-day peak was significant in the eastern EIO. The biweekly wind forcing being prominent in the eastern EIO [*Murty et al.*, 2002; Miyama *et al., 2005*], the 17-day peak is linked to direct wind forcing. Though a 28-day peak was seen in eastern EIO it was not significant. Thus, from the analysis of MSLA as well as the ADCP the presence of lower frequency Yanai wave could be inferred in the upper water column. This is at variance with the earlier observation as well as modeling studies which observed only the

higher frequency (mostly in the biweekly period) Yanai wave in the upper water column in the central EIO [*Reppin et al*., 1999; *Masumoto et al*., 2005; *Ogata et al*., 2008].

6. Summary and Conclusion

The presence of lower frequency Yanai waves in the upper pycnocline in the central EIO was inferred from the current meter and ADCP data at 77^0E and equator, along with MSLA data during 2003-2007. This is in contrast with the earlier observation as well as modeling studies that observed only the higher frequency (mostly in the biweekly period) Yanai wave in the upper water column in the central EIO. The lower frequency Yanai wave in the central EIO was seen during 2003, 2004, 2006 and 2007, which were the positive IOD years, while it was absent during the negative IOD year of 2005. During the positive IOD years, a strong meridional as well as vertical current shear was created by the westward flowing SEC and the eastward flowing south west monsoon current. During positive IOD years the barotropic conversion from MKE to EKE due to the cross-equatorial meridional current shear generates the lower frequency MRG wave while the higher baroclinic energy due to the vertical current shear supplies energy for the growth of MRG wave. The barotropic energy conversion to the mean flow and the negligible baroclinic energy conversion during the negative IOD year is not congenial for the generation of the lower frequency Yanai wave. The higher frequency Yanai wave, which was observed in the upper pycnocline was due to the direct wind forcing as mentioned by the earlier studies. During 2005 the higher frequency Yanai wave is not seen significant in the upper pycnocline. Irrespective of the positive or negative IOD years, the higher frequency Yanai wave signature alone was observed in the lower pycnocline. However, 47-day period oscillations were capable of generating resonance in the weakly stratified deeper ocean. In summary, during positive IOD years the upper water column dominantly resonates at the Yanai wave frequency due to the increased meridional shear and vertical stratification, while the deeper waters exhibits 47-day oscillations. During negative IOD year due to the lack of mean easterly wind and weakly stratified water column, the entire water column exhibited 47-day oscillations.

The present study, though utilized a long time-series current data, had only one negative IOD year and four IOD years in the study period. A detailed study with adequate in situ data consisting of normal as well as anomalous years is necessary to have a better understanding of the occurrence of Yanai wave in the central EIO and its interannual variability. A model simulation of IOD forcing that can provide a significant support to our observational findings is our future interest.

Acknowledgement

The authors wish to acknowledge Director, National Institute of Oceanography, Goa and Council of Scientific and Industrial Research (CSIR), New Delhi for all the support and encouragement. We thank the mooring team V. Fernando, A. Almeida, S. Khalap, S. Narayan and G. Mithun for their support by carrying out the mooring operations from onboard ORV Sagar Kanya. Authors Divya and Byju acknowledge CSIR for their fellowships. This is NIO contribution number XXXX.

REFERENCES

Addison, P. S. (2002), The illustrated wavelet transform handbook, *IOP publishing Ltd*., pages 6-63.

Bond, N. A., and G. A.Vecchi (2003), On the Madden Julian oscillation and precipitation in Oregon and Washington, *Weath. Forecast*., *18*, 600–613.

Bonjean, F., and G.S.E. Lagerloef (2002), Diagnostic Model and Analysis of the Surface Currents in the Tropical Pacific Ocean, *Journal of Physical Oceanography, Vol. 32, No. 10,* pages 2938-2954.

Chatterjee, P., and B. N. Goswami (2004), Structure, genesis and scale selection of the tropical quasi-biweekly mode, *Q. J. R. Meteorol. Soc., 130 (599),* 1171–1194.

Chen, T. C., and J.-M. Chen (1993), The 10–20 day mode of the 1979 Indian monsoon: Its relation with time variation of monsoon rainfall, *Mon. Weather Rev.*, *121,* 2465–2482.

Cox, M.D. (1980), Generation and propagation of 30 day waves in a numerical model of the Pacific, *J. Phys. Oceanogr., 10,* 217- 248.

Duvel, J. P., and J. Vialard (2007), Indo-Pacific Sea Surface Temperature Perturbations Associated with Intraseasonal Oscillations of the Tropical Convection, *Journal of Climate.*, *20***,** 3056-3082.

Emery, J. W., and Richard E. Thompson (1997), Data analysis methods in physical oceanography, *Pergamon*., pages 417 – 425.

Gutzler, D. S., and R. A. Madden (1989), Seasonal variations in the spatial structure of intraseasonal tropical wind fluctuations, *J. Atmos. Sci., 46,* 641-660.

Han, W.(2005), Origins and dynamics of the 90-day and 30–60-day variations in the equatorial Indian Ocean, *J. Phys. Oceanogr*., *35,* 708–728.

Harvey, R. R., and W. C. Patzert (1976), Deep current measurements suggest long waves in the eastern equatorial Pacific, *Science., 193,* 883-884.

Hirst, A., and K. M. Lau (1990), Intraseasonal and Interannual Variability in Coupled Ocean-Atmosphere Models, *J. Climate., 3,* 713-725.

Jochum, M., P. Malanotte-Rizzoli, and A. Busalacchi (2004a), Tropical instability waves in the Atlantic Ocean, *Ocean Modell., 7,* 145-163.

Jones, C., Waliser, D. E., Lau, K. M. and Stern, W (2004), The Madden Julian oscillation and its impact on northern hemisphere weather predictability, *Mon. Weath. Rev., 132,* 1462–1471.

Kelly, B. G., Steven D. Meyers, and James J. O'Brien (1995), On a generating mechanism for Yanai waves and the 25-day oscillation, *J. Geophys. Res.*, *Vol. 100, NO.C6,* Pages 10, 589-10, 612.

Kindle, J. C., and J. D. Thompson (1989), The 26 and 50 day oscillations in the western Indian Ocean: Model results, *J. Geophys. Res., 94 (C4),* 4721- 4736.

Lau, K. M., and Paul H. Chan (1988), Intraseasonal and Interannual Variations of Tropical Convection: A Possible Link between the 40–50 Day Oscillation and ENSO? *J.Atmos. Sci., 45,* 506-521.

Lau W., and Waliser D (2005), Intraseasonal Variability in the Atmosphere-Ocean Climate System, *(Springer–Praxis, Chichester, UK)*.

Legeckis. R. (1977), Long waves in the eastern equatorial Pacific ocean: A view from a geostationary satellite, *Science., 197,* 1179-1181.

LI, Chongyin., HU Ruijin and YANG Hui (2005), Intraseasonal Oscillation in the Tropical Indian Ocean*, Advances In Atmospheric Sciences*., *Vol. 22, No. 5,* 617–624.

Long, Z., and Li Chongyin (2002), Interannual variability of 30 – 60 day low frequency kinetic energy in the lower tropical atmosphere, *Chinese J. Atmos. Sci*.

Luyten, J. R., and Dean H. Roemmich (1982), Equatorial currents at semi-annual period in the Indian ocean, *J. Phys.Oceanogr., 12,* 406-413.

Madden R. A. (1986), Seasonal variations of the 40-50 day oscillation in the tropics, *J. Atmos. Sci., 43,* 3138-3158.

Madden R. A., and P. R. Julian (1971), Detection of a 40-50 day oscillation in the zonal wind in the tropical Pacific, *J.Atmos. Sci*., *28,* 702-708.

Madden, R. A., and P. R. Julian (1972), Description of global-scale circulation cells in the tropics with a 40– 50 day period, *J. Atmos. Sci., 29,* 1109–1123.

Masumoto, Y., Hideaki Hase, Y. Kuroda, H. Matsuura and K. Takeuchi (2005), Intraseasonal variability in the upper layer currents observed in the eastern equatorial Indian Ocean, *Geophys. Res. Lett., Vol.32,* L02607, doi:10.1029/2004GL021896.

Mcphaden, M.J. (1982), Variability in the central equatorial Indian Ocean Part I: Ocean dynamics, *J.Mar.Res.,40,*157-176.

McPhaden, M. J. (1999), The genesis and evolution of the 1997–98 El Nin`o, *Science.,* 283, 950–954.

Meyers, S. D., B. G. Kelley and James J. O'brien (1993), An introduction to wavelet analysis in oceanography and meteorology: with application to dispersion of Yanai Waves, *Mon. Wea.Rev., 121,* 2858-2866.

Miyama, T., J. P. Mccreary, Debasis Sengupta and Retish Senan (2005), Dynamics of biweekly oscillations in the equatorial Indian Ocean, *J. Phys. Oceanogr., 36,* 827- 846.

Moore, D. W., and J. P. Mccreary (1990), Excitation of intermediate frequency equatorial waves at a western ocean boundary: With application to observations from the Indian Ocean, *J. Geophys. Res., 95(C4),* 5219- 5231.

Murakami, T., and M. Frydrych (1974), On the preferred period of upper wind fluctuations during the summer monsoon, *J. Atmos. Sci., 31,* 1549–1555.

Murty, V.S.N., A. Suryanarayana, M.S.S.Sarma, A.Tilvi, Vijayan Fernando, G. Nampoothiri, Areef Sardar, D. Gracias and Sadashiv Khalap (2002), Current meter moorings along the equator

Vertical current structure variability at equator, 93^{o}E during February to December 2000, *PORSEC 2002 BALI proceedings*.

Murty, V.S.N, M.S.S. Sarma, A. Suryanarayana, D. Sengupta , A. S. Unnikrishnan ,V. Fernando, A. Almeida, S. Khalap, A. Sardar, K. Somasundar and M. Ravichandran (2005), Indian Moorings: Deep-sea current meter moorings in the Eastern Equatorial Indian Ocean, *CLIVAR Exchanges*., *Vol.11*; 5-8p.

Numaguti, A. (1995), Characteristics of 4- to 20-day period disturbances observed in the equatorial Pacific during the TOGA COARE IOP, *J. Meteorol. Soc. Japan., 73,* 353– 377.

Ogata, T., Hiderharu Sasaki, V.S. N. Murty, M.S.S.Sarma and Yukio Masumoto (2008), Intraseasonal meridional current variability in the eastern equatorial Indian Ocean, *J.Geophys. Res*., *Vol.113*, *C070377,* doi:10.1029/2007JC004331.

O'Neill, K. (1984), Equatorial velocity profiles, part I, Meridional components, *J. Phys. Oceanogr., 14,* 1829-1841.

Pond, S., and G.L. Pickard (1983), Introduction to dynamical oceanography, Pergamon Press, New York 241pp.

Reverdin, G., and J. Luyten (1986), Near surface meanders in the equatorial Indian Ocean, *J. Phys.Oceanogr., 16,* 1088- 1100.

Reppin, J., Friedrich A. Schott, and Jurgen Fischer and Detlef quadfasel (1999), Equatorial currents and transports in the upper central Indian Ocean: Annual cycle and interannual variability, *J. Geophys. Res., Vol.104, NO.C7*, Pages 15,495-15,514.

Ripa, P., and S. P. Hayes (1981), Evidence for Equatorial Trapped waves at the Galapago Islands, *J. Geophys. Res., VOL.86, NO.C7,* Pages 6509-6516.

Schott, F., J. Reppin, J.Fischer and D.Quadfasel (1994), Currents and transports of the monsoon current south of Sri lanka, *J.Geophys.Res., 99,* 25127-25141.

Sengupta, D., Retish Senan and B. N. Goswami (2001), Origin of intraseasonal variability of circulation in the tropical central Indian Ocean, *Geophys. Res. Lett., Vol. 28, NO.7* Pages 1267-1270.

Sengupta, D., Retish Senan, V. S. N. Murty and V. Fernando (2004), A biweekly mode in the equatorial Indian Ocean, *J. Geophys. Res., 109, C10003*, doi: 10.1029/2004JC002329.

Sobel, A. H., Eric D. Maloney, Gilles Bellon and Dargan M. Frierson (2008), The role of surface heat fluxes in tropical intraseasonal oscillations, *Nature Geoscience., Vol 1*, Pages 653-655.

Tsai, P. T. H., James J. O'Brien and Mark E. Luther (1992), The 26-day oscillation observed in the satellite sea surface temperature measurements in the equatorial western Indian Ocean, *J. Geophys. Res.*, *Vol.97, No.C6,* Pages 9605-9618.

Waliser, D. E., R. Murtugudde, and L. Lucas (2003), Indo-Pacific Ocean response to atmospheric intraseasonal variability. Part I: Austral summer and the Madden–Julian oscillation. *J. Geophys. Res*., *108, 3160,* doi:10.1029/2002JC001620.

Wang B., and Xie X (1998), Coupled modes of the warm pool climate system Part I: The role of air-sea interaction in maintaining Madden-Julian oscillation, *Journal of Climate*., *11:* 2116–2135.

Weisberg, R. H., and A. M. Horigan (1981), Low-frequency variability in the equatorial Atlantic, *J. Phys. Oceanogr*., *11,* 913–920.

Weisberg, R. H., A. M. Horrigan and C. Colin (1979), Equatorially trapped Rossby gravity wave propagation in the Gulf of Guinea, *J. Mar.Res., Vol. 37, 1*.

Wheeler, M., and G. N. Kiladis (1999), Convectively coupled equatorial waves: Analysis of clouds and temperature in the wave number-frequency domain, *J. Atmos. Sci.*, *56,* 374-399.

Woodberry, K. E., Mark E. Luther and James J. O'brien (1989), The wind driven seasonal circulation in the southern tropical Indian Ocean, *J. Geophys.Res., Vol. 94, NO.C12,* Pages 17985-18002.

Wunsch. C., and A.E, Gill (1976), Observations of equatorially trapped waves in the Pacific sea level variations, *Deep Sea Res*., *23,* 371-390.

Yu, J. Y., and W. T. Liu (2001), Seasonal-to-interannual modulations of tropical Instability waves and the their coupling with the atmosphere, *Proceedings of the 12th Symposium On Global Change and Climate Variations*., 14-18 January 2001, Albuquerque, New Mexico, 50-53.

Table captions

Table.1. Period of deployment, retrieval and data availability of the RCM and ADCP.

Table. 2. Argo data used for calculating the annual mean temperature (^{o}C), salinity (psu) and sigma-t (kg/m^{3}) profiles.

Table 3. Prominent peaks in the meridional current velocity from ADCP data during 19 October 2004 to 25 June 2006 obtained from chi-squared distribution with 95% CL. N.A indicates no significant peak.

Table 4. Depth averaged density gradient and static stability computed from Argo data during the period 2003 to 2007.

Table 5. Prominent peaks in the meridional current velocity from RCM data during three retrieval periods of 2003-04, 2004-05 and 2006-07 obtained from chi-squared distribution with 95% CL.

Figure Captions

Figure 1. The schematic diagram showing the availability of ADCP as well as current meter (RCM) data at 77^{0}E, equator during the period September, 2003 to December, 2007.

Figure 2. The study region (mooring site) at 77^{0}E, equator (white star), western (blue box), central (white box), and eastern (magenta box) EIO. The shading is the zonal current (m/s) for the month of October, 2006 (positive IOD period) derived from OSCAR data (see text for details). The white broken line represents the zero zonal current velocity.

Figure 3. The annual mean salinity (blue), temperature (red) and sigma-t (black) profiles at 77^{o}E and equator from Argo data during (a) positive IOD year, 2006 and (b) negative IOD year, 2005. The shaded portion is the region (96-120m) where the signature of higher frequency Yanai wave was inferred during 2003 to 2007.

Figure 4. Energy spectrum of meridional current velocity ((cm^{2}/s^{2})/day) of ADCP for the period 19 October 2004 to 25 June 2006 averaged over the depth 48 to 88m (upper panel) and 96 to 120m depth (lower panel). Dark red in the colour bar stands for maximum energy and dark blue for minimum energy. The black ellipses show the significant energy levels of the spectra.

Figure 5. Energy spectrum of meridional current velocity ((cm^2/s^2)/day) of RCM for the period 2003-2004 at (a) 150m, (b) 300m, (c) 500m, (d) 1000m and (e) 4000m depth . Dark red in the colour bar stands for maximum energy and dark blue for minimum energy. The black ellipses show the significant energy levels of the spectra.

Figure 6. Energy spectrum of meridional current velocity ((cm^2/s^2)/day) of RCM for the period 2004-2005 at (a) 500m, (b) 2000m and (c) 4000m depth. Dark red in the colour bar stands for maximum energy and dark blue for minimum energy. The black ellipses show the significant energy levels of the spectra.

Figure 7. Energy spectrum of meridional current velocity ((cm^2/s^2)/day) of RCM for the period 2006-2007 at (a) 450m, (b) 550m, (c) 800m, (d) 1000m and (e) 4000m depth. Dark red in the colour bar stands for maximum energy and dark blue for minimum energy. The black ellipses show the significant energy levels of the spectra.

Figure 8. The schematic diagram of (a) climatological vertical stratification (2003-2007) of the water column in the study region from the Argo data regridded to 2° X 2° from 76^0E-78^0E and 1°N-1°S and the vertical distribution of lower and higher frequency Yanai wave with 95% CL during (b) positive IOD years of 2003, 2004, 2006 and 2007 and (c) negative IOD year of 2005.

Figure 9. CS with 95% and above CL of daily meridional wind stress from QuikSCAT in the central EIO (75^0E-80^0E averaged and equator) during (a) 2003, (b) 2004, (c) 2005, (d) 2006 and (e) 2007.

Figure 10. VP of daily meridional wind stress from QuikSCAT in the central EIO (75^0E-80^0E averaged and equator) during (a) 2004 and (b) 2007.

Figure 11. Weekly Dipole Mode Index based on Sea Surface Temperature (NOAA O1 SST Ver. 2, 1982-2008) during 2003-2007 (light grey line). Black line represent two month running mean of the SST index. The shaded area is the negative IOD year of 2005. The vertical red bars represent the monthly mean of the positive DMI months and the black bars represent the annual mean DMI for the respective years.

Figure 12. Zonal current velocity (m/s) (shading) from OSCAR overlaid with wind vector

(speed in m/s) from QuikSCAT averaged for the month of October during (a) positive IOD year, 2006 and (b) negative IOD year, 2005 in the Indian Ocean. The difference in zonal current shear (s^{-1}) between 2006 and 2005 for the month of October (c) and the time average (May-November) of barotropic (black line), baroclinic (red line) and total (green line) energy conversions (kg/ms^3) during 2003 to 2007 in the central EIO (averaged over 75^0E-80^0E and 3^0N-3^0S) (d). The rectangular box represents the area of generation of lower frequency Yanai wave in the central EIO.

Figure 13. CS of the antisymmetric MSLA after the removal of the seasonal signature from 19 Oct 2004 to 25 Jun 2006 at 3^0N (top panel) in western EIO [50^0E-60^0E averaged], (middle panel) in central EIO [70^0E-80^0E averaged] and (bottom panel) in eastern EIO [90^0E-100^0E averaged]. Red line represents 95% CL.

TABLE 1. Period of deployment, retrieval and data availability of the RCM and ADCP.

Data source	Deployment Date	Retrieval Date	Period of data availability		Depth (m)	Data gap
			Starting Date	Ending Date		
RCM	10 September, 2003	17 October, 2004	12 September, 2003	16 October, 2004.	150	31 Dec, 2003 27 and 28 Mar, 2004 10-13 Jul,2004
					300	7,8 and 18 Feb, 2004 31 Mar 2004 1 Apr, 2004 10 and 11, May, 2004 12 Aug, 2004
					500	22 and 29, Nov, 2003 6,13,19 and 20 Jan, 2004 1 and 7, Oct, 2004
					1000	21-25 Oct, 2003 1, 3 and 9, Nov, 2003 8 and 9, Jan, 2004 **(Data upto 20 Apr, 2004 is available)**
					2000	3-5 and 10-15 Oct, 2003 4-8 and 15-18, Nov,2003 8, 12-14 and 18 Dec, 2003 3, 5-16, 19-21, 26, 29 and 30 Jan, 2004 3-18 Feb, 2004 12-14, 24-31, Mar, 2004 6-8 Apr, 2004 9 May, 2004 21-30 May, 2004 3, 4, 18 and 19 Jun, 2004 1-14 Jul, 2004 19-23 Aug, 2004 5-9 Oct, 2004 **(Not used)**
					4000	No gap
	18 October, 2004	25 September, 2006	20 October, 2004	28 December, 2005.	300	Only 14 day data available 20 Oct – 2 Nov, 2004 **(Not used)**
					500	25 Dec, 2004 14 Feb, 2005 7 and 8, Apr, 2005 15 – 30 May, 2005 15 Jun, 2005 16 and 17 Dec, 2005
					2000	No gap
					4000	No gap
	27 September, 2006	May, 2008	29 September, 2006	6 December, 2007.	450	No gap
					550	No gap
					800	No gap
					1000	No gap
					2000	Only 59day data available 29 Sep-28 Nov,2006 **(Not used)**
					4000	No gaps
ADCP	18 October, 2004	25 September ,2 006	19 October, 2004	25 June, 2006.	48	10-15,17-28 Jan, 4-17 May, 5-14 Jun,12-23 Jul, 22-27 Sep, 22-27 Nov, 24-31 Dec 2005, 1-11 Jan, 6- 17 Feb, 19-31 Mar, 23-31 May 2006
					56	19-27 Jan, 4-17 May, 9-12 Jun, 9-11,13-24 Jul, 6-10 Aug, 22-27 Sep, 24-31 Dec 2005, 1-11 Jan, 14-24 Feb, 23-31 May 2006
					64	4-15 May, 13-24 Jul, 22-26 Sep, 24-32 Dec 2005, 10-21 Feb, 27-31 May 2006
					72	4-15 May, 14-19 Jul, 25-31 Dec 2005, 10-21 Feb, 27-31 May 2006
					80	11-17 May, 14-19 Jul, 25-32 Dec 2005, 10-21 Feb, 27-31 May 2006
					88	4-9 May, 14-19 Jul, 25-31 Dec 2005, 1-9 Jan, 10-21 Feb, 27-31 May 2006
					96	9-12 Dec 2004, 10-14 Jan, 9-13 Feb, 4-16 Jun, 11-17, 26-31 Jul, 1-7 Aug, 23-31 Dec 2005, 1-6, 8-11 Jan, 12-18 Feb, 27-29 May, 1,6,9 Jun 2006
					104	10-20 Nov, 28-31 Dec 2004, 23-28 Feb, 19-25 Apr, 25-31 Dec 2005, 1-9,25-31 Jan, 10-18 Feb, 29-31 May 2006
					112	6-14,16-23 Nov, 28-31 Dec 2004, 23-28 Feb, 19-25 Mar 2005, 4-6,11-13 May, 25-31 Dec 2005, 25-31 Jan, 11-18 Feb,3-4, 30-31 May, 16-18 May 2006
					120	10-24 Nov, 12-18 Dec 2004, 22-28 Feb, 19-28 Mar, 26-30 Apr, 18-22,26-31 Aug, 3- 15 Sep, 16- 19,25-29 Oct, 1-4,12-16 Nov, 15- 20, 26-27 Dec 2005, 1-5,13-17,19- 31 Jan, 11-18 Feb, 21-24 Apr, 2-4 May, 8-9,17, 21 Jun 2006

TABLE 2. Argo data used for calculating the annual mean temperature (^{o}C), salinity (psu) and sigma-t (kg/m^{3}) profiles.

Years of Argo profile data	Total no: of profiles used	Argo ID	No: of profiles used within 76°E-78°E longitude and 1°N-1°S latitude from each Argo ID
2003	10	D2900228	5
		R2900233	1
		D2900101	1
		R2900233	1
		D1900183	1
2004	10	D2900229	1
		D1900188	1
		D1900158	8
2005	27	D2900103	6
		R2900493	3
		D2900532	3
		D2900230	5
		D2900100	6
		D1900158	1
		D2900570	4
2006	30	D2900567	2
		D2900103	4
		D2900230	2
		D2900570	5
		D2900679	17
2007	42	R2900678	27
		D4900511	1
		R2900678	13
		R2900560	1

TABLE 3. Prominent peaks in the meridional current velocity from ADCP data during 19 October 2004 to 25 June 2006 obtained from chi-squared distribution with 95% CL. N.A indicates no significant peak.

Depth (m)	Chi-squared distribution peaks of meridional velocity from ADCP (cm/s) in days
48	26, 12
56	26, 12
64	26
72	26
80	N.A
88	26
96	19
104	19
112	15
120	22

TABLE 4. Depth averaged density gradient and static stability computed from Argo data during the period 2003 to 2007.

Years	Depth averaged density gradient (kg/m^4)			Depth averaged static stability ($x\ 10^{-6}\ m^{-1}$)		
	Depth range (m)			Depth range (m)		
	48-88	96-120	150-1000	48-88	96-120	150-1000
2003	0.0333	0.0111	0.0046	-478.439	-95.106	-19.698
2004	0.0429	0.0285	0.0031	-562.64	-253.798	-14.955
2005	0.0309	0.0341	0.0023	-454.951	-301.682	-10.619
2006	0.0367	0.0333	0.0029	-515.781	-295.957	-13.402
2007	0.0368	0.0347	0.0042	-517.055	-302.365	-19.902

TABLE 5. Prominent peaks in the meridional current velocity from RCM data during three retrieval periods of 2003-04, 2004-05 and 2006-07 obtained from chi-squared distribution with 95% CL.

Deployment -Recovery period	Depth (m)	Meridional current velocity from RCM Chi-squared distribution peaks (days)
2003-04	150	28,10
	300	28,7
	500	21,11
	1000	23,7
	4000	47
2004-05	500	47,16
	2000	47
	4000	47
2006-07	450	21
	550	21,13
	800	28, 13
	1000	28,16
	4000	47

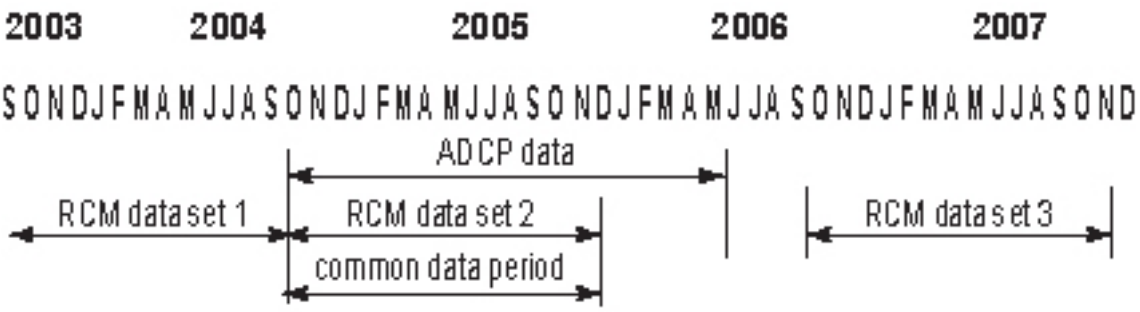

Figure 1. The schematic diagram showing the availability of ADCP as well as current meter (RCM) data at 77°E, equator during the period September, 2003 to December, 2007.

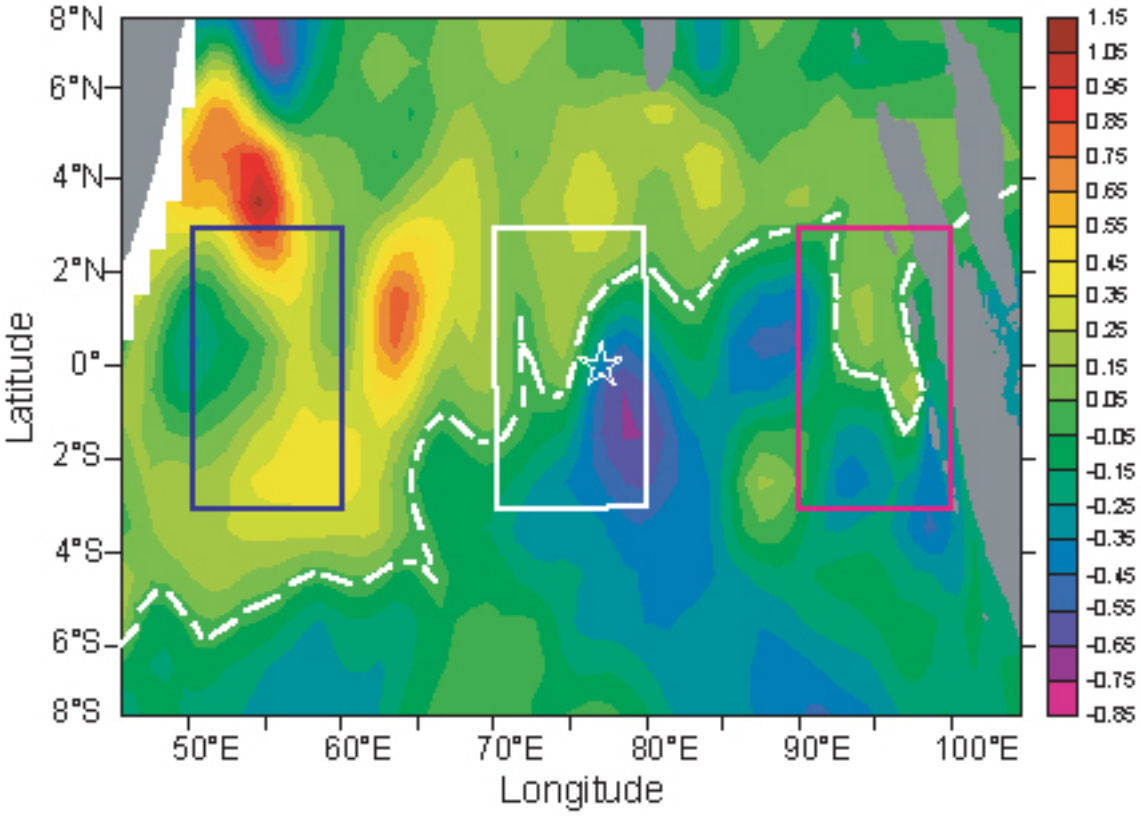

Figure 2. The study region (mooring site) at 77°E, equator (white star), western (blue box),central (white box) and eastern (magenta box) EIO. The shading is the zonal current (m/s) for the month of October, 2006 (positive IOD period) derived from OSCAR data (see text for details). The white broken line represents the zero zonal current velocity.

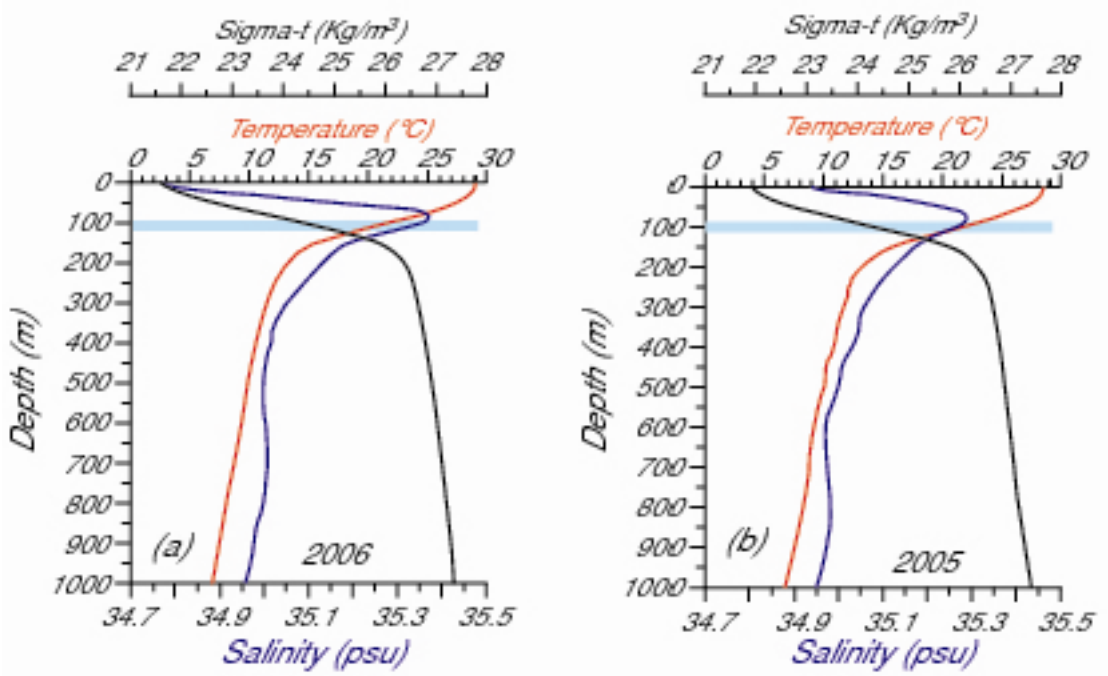

Figure 3.The annual mean salinity (blue), temperature (red) and sigma-t (black) profiles at 77°E and equator from Argo data during (a) positive IOD year, 2006 and (b) negative IOD year, 2005. The shaded portion is the region (96-120m) where the signature of the higher frequency Yanai wave was inferred during 2003 to 2007.

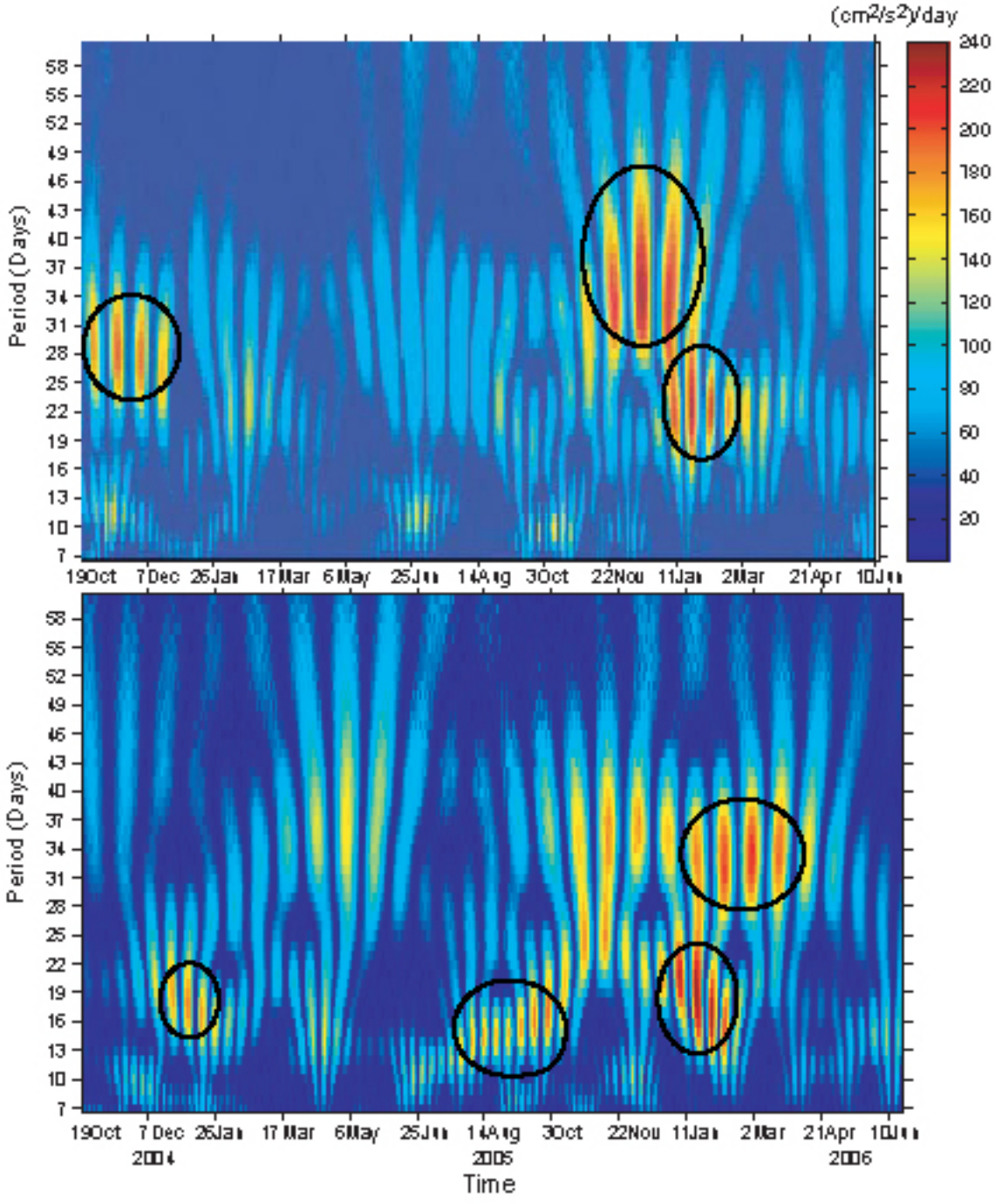

Figure 4. Energy spectrum of meridional current velocity ((cm^2/s^2)/day) of ADCP for the period 19 October 2004 to 25 June 2006 averaged over the depth 48 to 88m (upper panel) and 96 to 120m depth (lower panel). Dark red in the colour bar stands for maximum energy and dark blue for minimum energy. The black ellipses show the significant energy levels of the spectra.

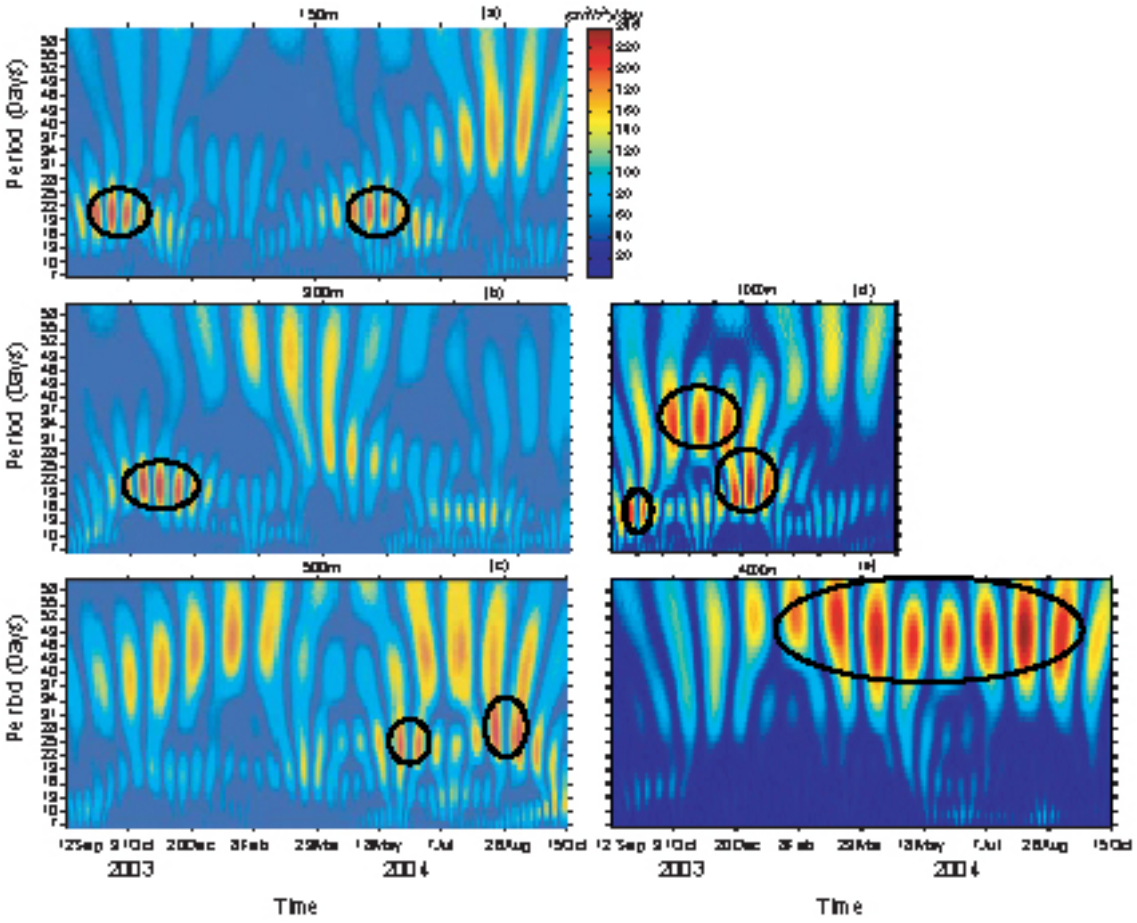

Figure 5. Energy spectrum of meridional current velocity ((cm^2/s^2)/day) of RCM for the period 2003-2004 at (a) 150m, (b) 300m, (c) 500m, (d) 1000m and (e) 4000m depth. Dark red in the colour bar stands for maximum energy and dark blue for minimum energy.The black ellipses show the significant energy levels of the spectra.

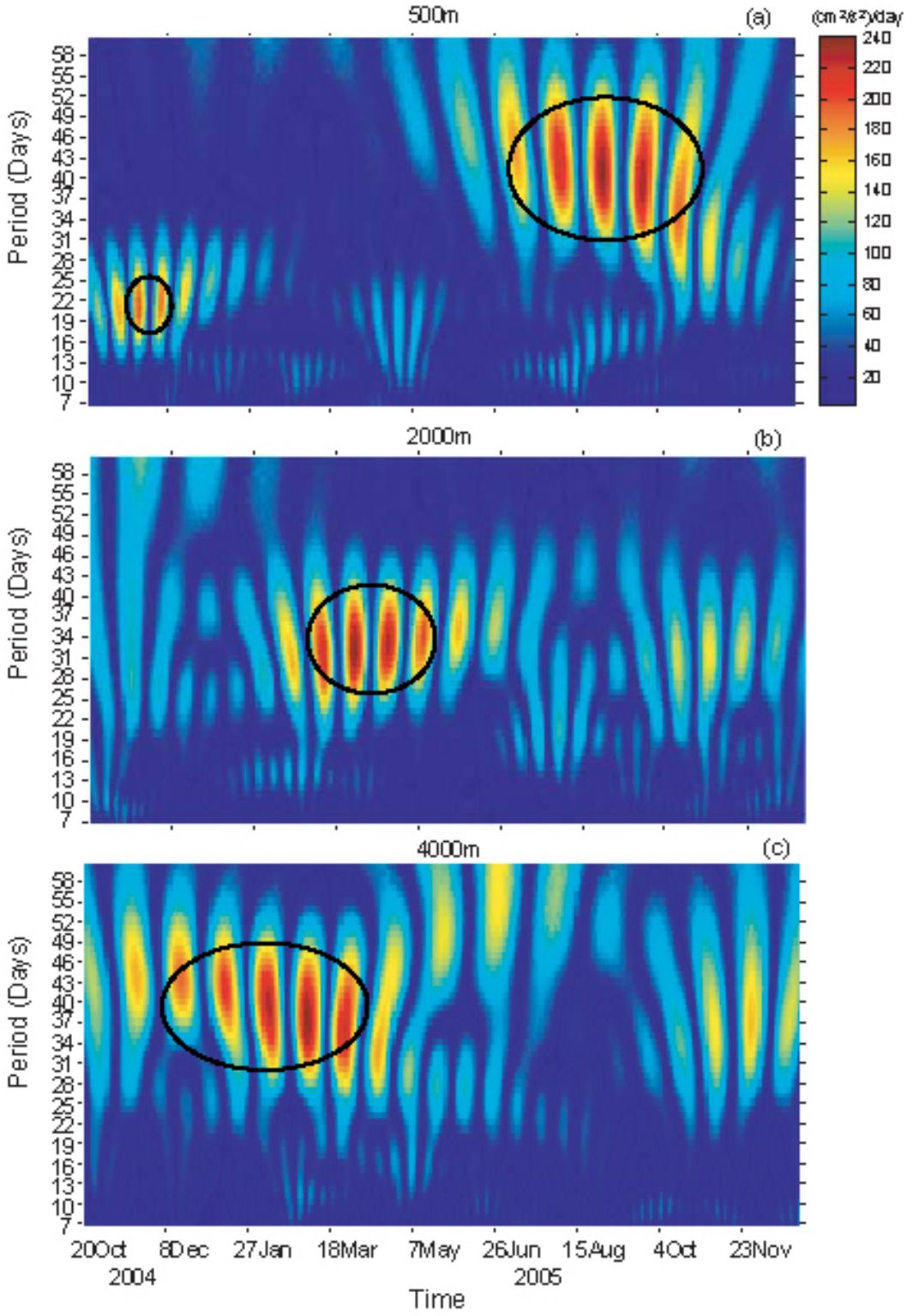

Figure 6. Energy spectrum of meridional current velocity ((cm^2/s^2)/day) of RCM for the period 2004-2005 at (a) 500m, (b) 2000m and (c) 4000m depth. Dark red in the colour bar stands for maximum energy and dark blue for minimum energy.The black ellipses show the significant energy levels of the spectra.

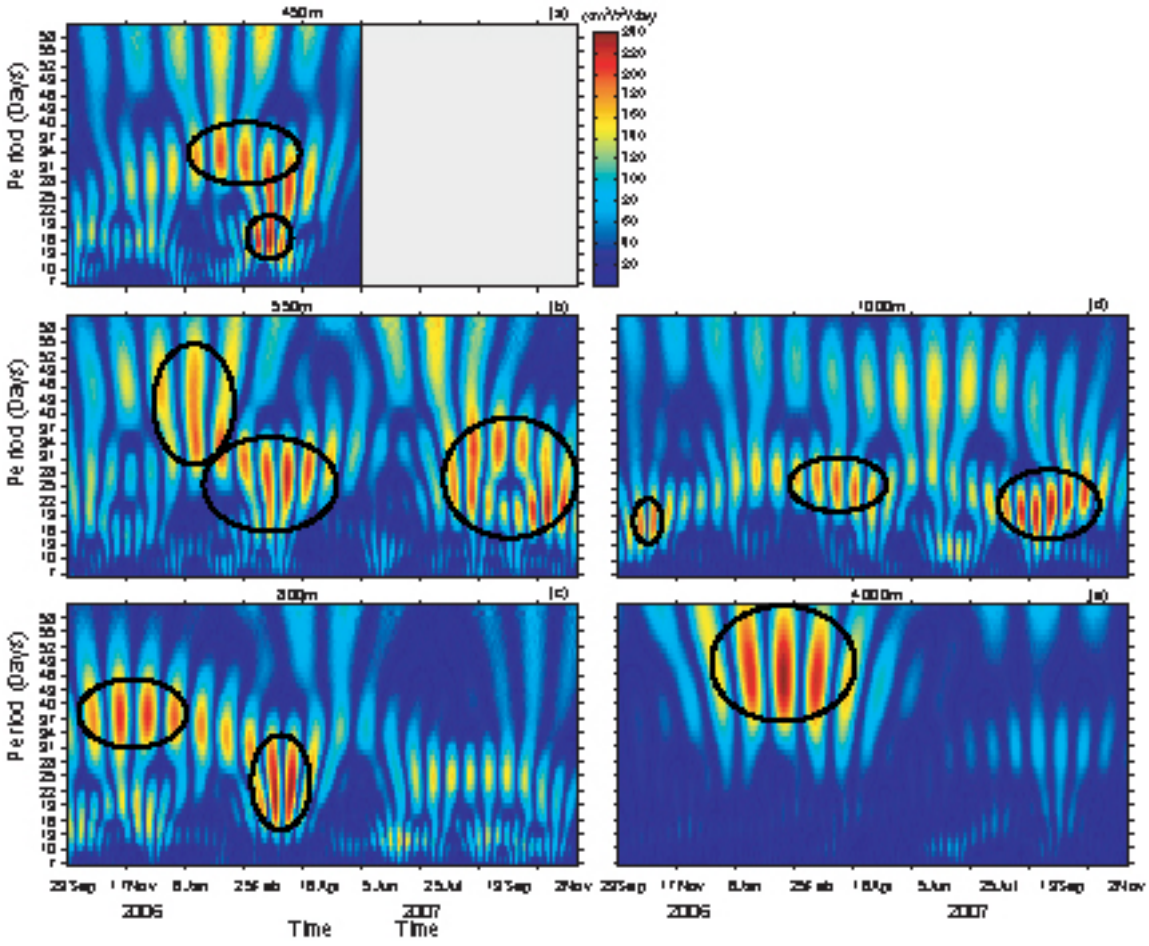

Figure 7. Energy spectrum of meridional current velocity ((cm^2/s^2)/day) of RCM for the period 2006-2007 at (a) 450m, (b) 550m, (c) 800m, (d) 1000m and (e) 4000m depth. Dark red in the colour bar stands for maximum energy and dark blue for minimum energy.The black ellipses show the significant energy levels of the spectra.

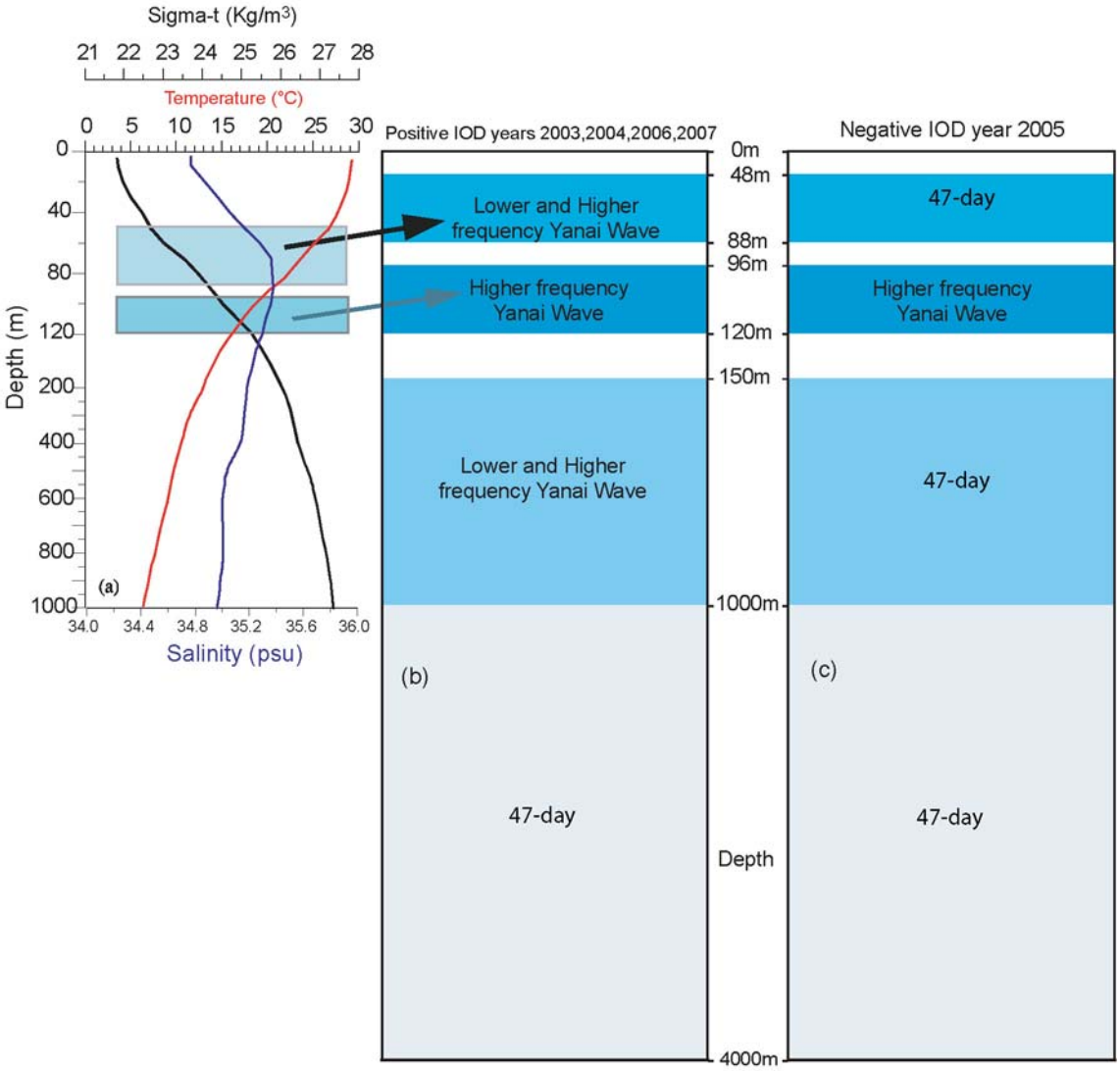

Figure 8. The schematic diagram of (a) climatological vertical stratification (2003-2007) of the water column in the study region from the Argo data regridded to 2° x 2° from 76°E-78°E and 1°N-1°S and the vertical distribution of lower and higher frequency Yanai wave with 95% CL during (b) positive IOD years of 2003, 2004, 2006 and 2007 and (c) negative IOD year of 2005.

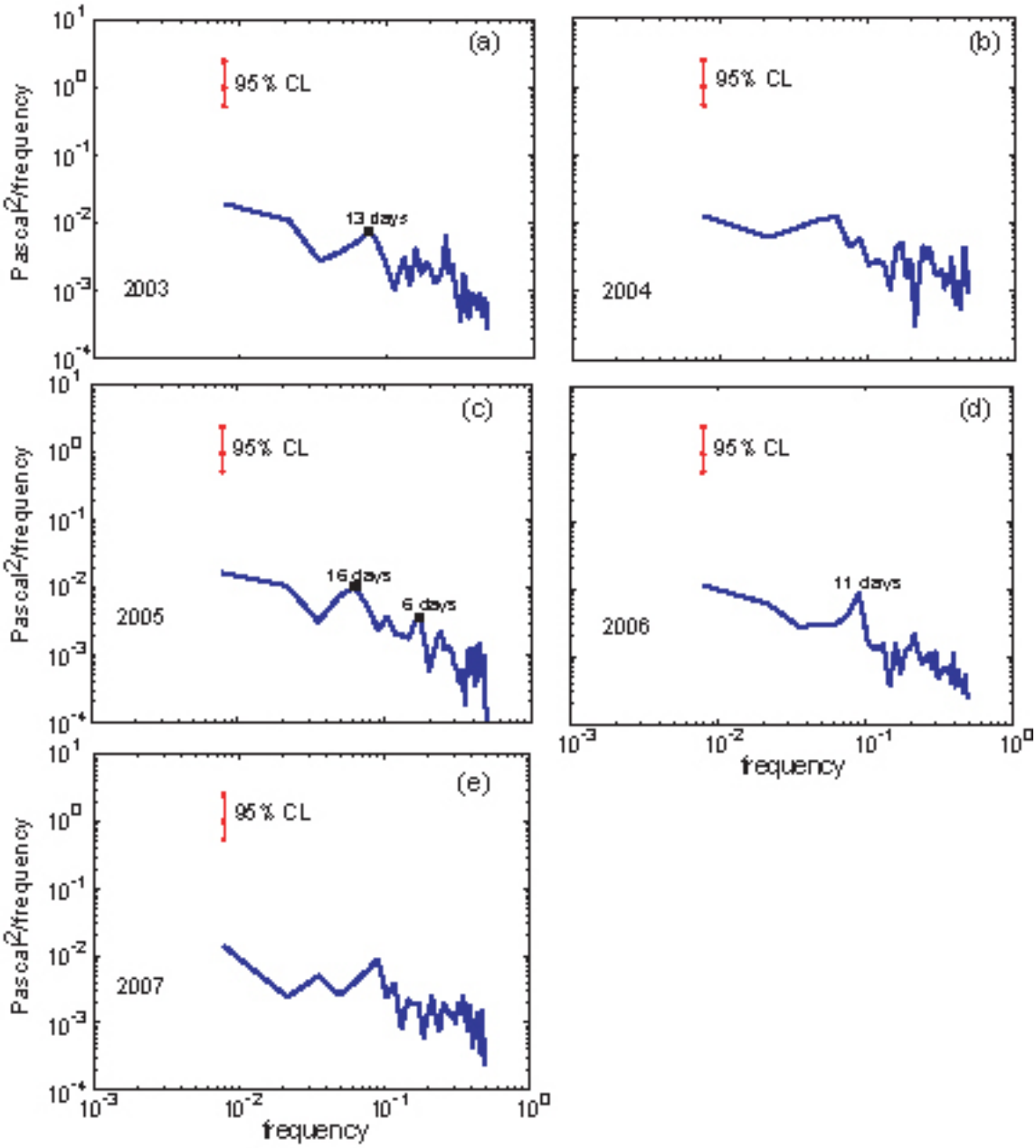

Figure 9. CS with 95% and above CL of daily meridional wind stress from QuikSCAT in the central EIO (75°E-80°E averaged and equator) during (a) 2003, (b) 2004, (c) 2005, (d) 2006 and (e) 2007.

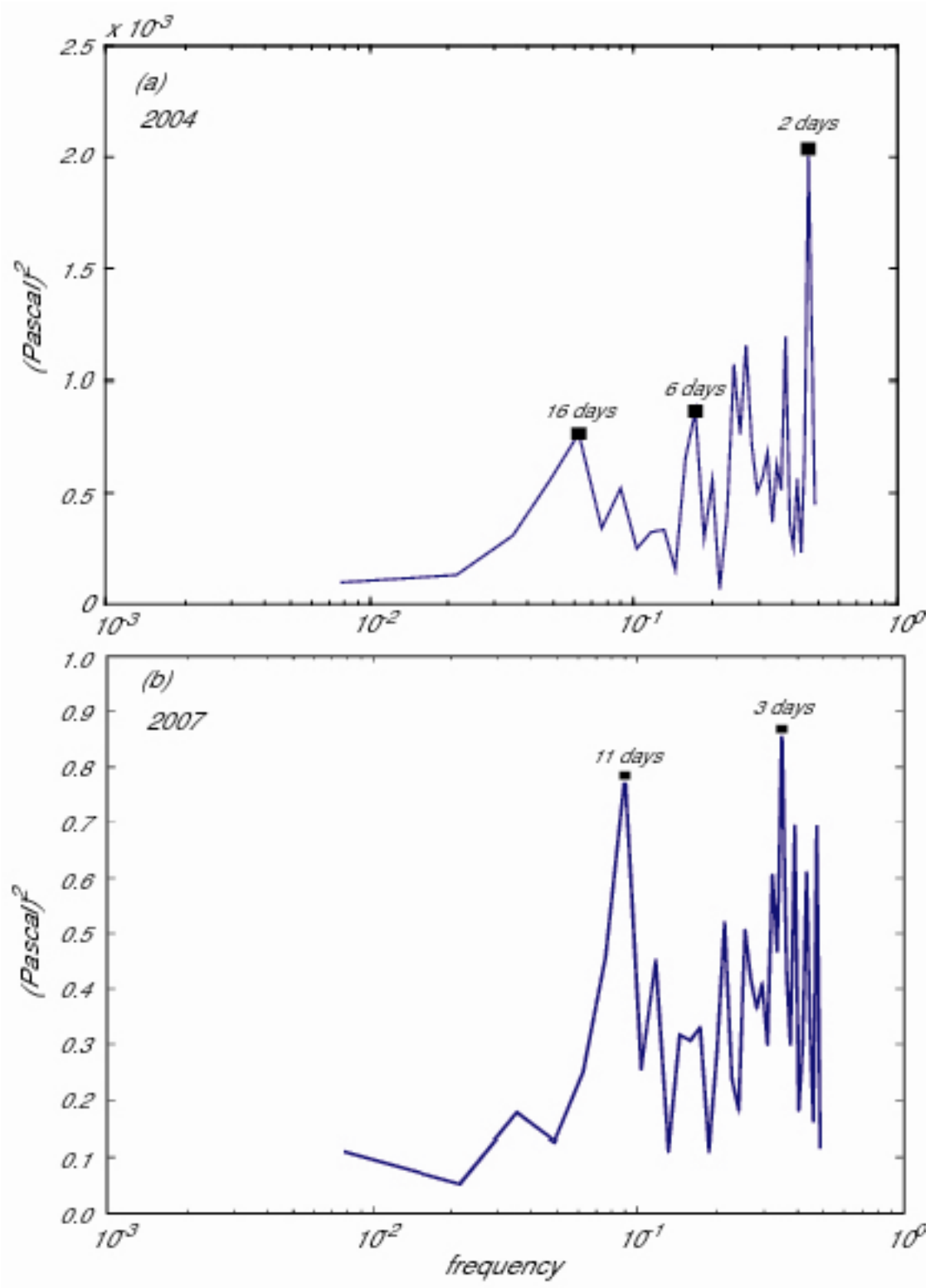

Figure 10. VP of daily meridional wind stress from QuickSCAT in the central EIO (75°E-80°E averaged and equator) during (a) 2004 and (b) 2007

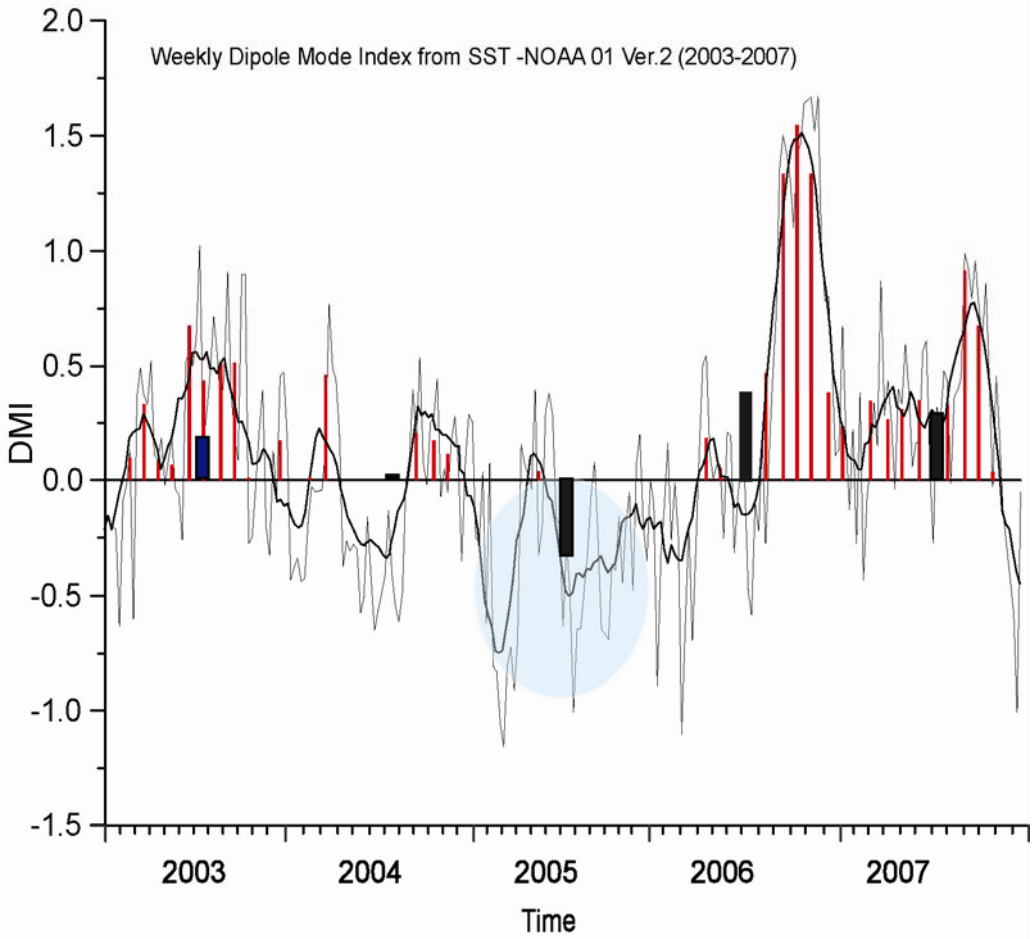

Figure 11. Weekly Dipole Mode Index based on the Sea Surface Temperature (NOAA O1 SST Ver. 2, 1982-2008) during 2003-2007 (light grey line). Black line repesent two month running mean of the SST index. The shaded area is the negative IOD year of 2005. The vertical red bars represent the monthly mean of the positive DMI months and the black bars represent the annual mean DMI for the respective years.

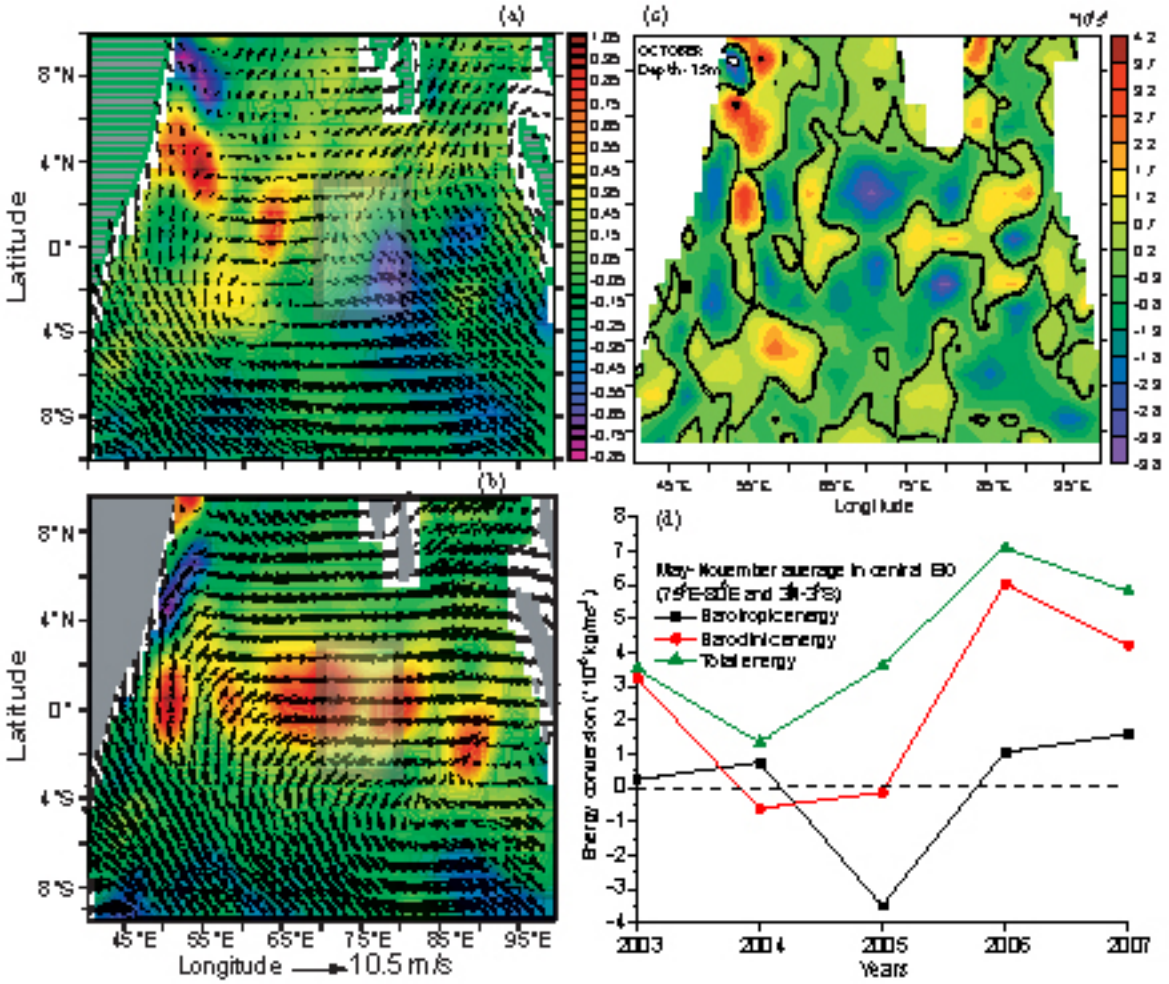

Figure 12. Zonal current velocity (m/s) (shading) from OSCAR overlaid with wind vector (speed in m/s) from QuikSCAT averaged for the month of October during (a) positive IOD year, 2006 and (b) negative IOD year, 2005 in the Indian Ocean. The difference in zonal current shear (s^{-1}) between 2006 and 2005 for the month of October (c) and the time average (May-November) of barotropic (black line), baroclinic (red line) and total (green line) energy conversions (kg/ms^3) during 2003 to 2007 in the central EIO (averaged over 75°E-80°E and 3°N-3°S) (d).The rectangular box represents the area of generation of lower frequency Yanai wave in the central EIO.

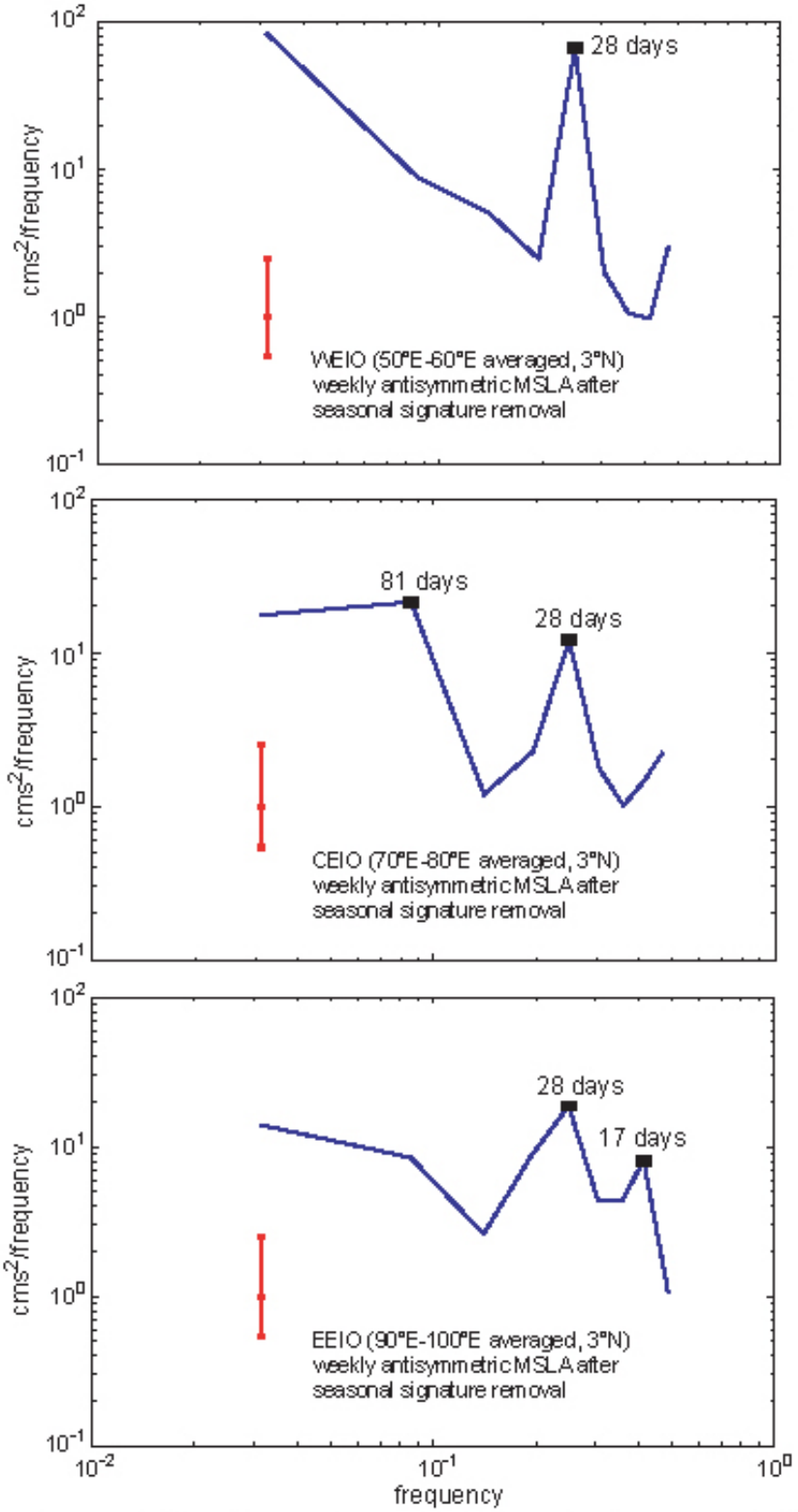

Figure 13. CS of the antisymmetric MSLA after the removal of the seasonal signature from 19 Oct 2004 to 25 Jun 2006 at 3°N (top panel) in western EIO [50°E-60°E averaged], (middle panel) in central EIO [70°E-80°E averaged] and (bottom panel) in eastern EIO [90°E-100°E averaged]. Red line represents 95% CL.